INVITED PAPER

Three-Dimensional Optical Sensing and Visualization Using Integral Imaging

The current state-of-the art, potential applications of integral imaging, recent research results, and potential applications are discussed.

By Myungjin Cho, Mehdi Daneshpanah, *Member IEEE*, Inkyu Moon, and Bahram Javidi, *Fellow IEEE*

ABSTRACT | Three-dimensional (3-D) optical image sensing and visualization technologies have been researched extensively for different applications in fields as diverse as entertainment, medical sciences, robotics, manufacturing, and defense. In many instances, the capabilities of 3-D imaging and display systems have revolutionized the progress of these disciplines, enabling new detection/display abilities that would not have been otherwise possible. As one of the promising methods in the area of 3-D sensing and display, integral imaging offers passive and relatively inexpensive way to capture 3-D information and to visualize it optically or computationally. The integral imaging technique belongs to the broader class of multiview imaging techniques and is based on a century old principle which has only been resurrected in the past decade owing to advancement of optoelectronic image sensors as well as the exponential increase in computing power. In this paper, historic and physical foundations of integral imaging are overviewed; different optical pickup and display schemes are discussed and system parameters and performance metrics are described. In addition, computational methods for reconstruction and range estimation are presented and several applications including 3-D underwater imaging, near infra red passive sensing, imaging in photon-starved environments, and 3-D optical microscopy are discussed among others.

KEYWORDS | Computational volumetric reconstruction; integral imaging; 3-D visualization

I. INTRODUCTION

New technologies that can be used to enhance sensing and visualization of real-world objects are always in demand. Acquiring information through imaging has always been a prominent approach for such purposes. In recent years, there has been an increased interest among researchers to develop 3-D imaging technologies that can provide information-rich imagery for application in disciplines as diverse as entertainment, medical sciences, robotics, manufacturing, and defense [1]–[3]. In many instances, the capabilities of 3-D imaging and display systems have revolutionized the progress of these disciplines, enabling new detection abilities that would not have been otherwise possible.

As opposed to traditional 2-D imaging, 3-D sensing technologies can potentially capture the structural information of the target as well as its texture. Many of the recent improvements in this area have been made possible in part by the advancement of optoelectronic display and image sensors, in addition to the exponential increase in computing power.

Integral imaging is a promising approach in the area of 3-D sensing and display. Historical origins of integral imaging can be traced back to Sir Wheatstone in 1828 [4] who introduced a stereoscopic viewing device known as "mirror stereoscope" [5] which operates based on the

Manuscript received April 26, 2010; revised August 6, 2010; accepted October 9, 2010. Date of publication December 3, 2010; date of current version March 18, 2011.
M. Cho and M. Daneshpanah equally contributed to this work.
M. Cho, **M. Daneshpanah**, and **B. Javidi** are with the Department of Electrical and Computer Engineering, University of Connecticut, Storrs, CT 06269-2157 USA (e-mail: yammako@engr.uconn.edu; mehdi@engr.uconn.edu; bahram.javidi@uconn.edu).
I. Moon is with the School of Computer Engineering, Chosun University, Gwangju 501-759, South Korea (e-mail: inkyu.moon@chosun.ac.kr).
Digital Object Identifier: 10.1109/JPROC.2010.2090114

principle of disparity. A major step was taken by Nobel laureate G. Lippmann with invention of integral photography in 1908 [6]. Besides early follow ups on Lippmann's integral photography [7]–[11], there was no substantial activity in this field for the rest of the twentieth century due to limitations of optical detectors and unavailability of mature plastic lens making technologies.

In the past decade, however, the principles of integral photography have been resurrected and developed by leveraging advancements in optoelectronic sensors like complementary metal–oxide–semiconductor (CMOS) and charge-coupled devices (CCDs), display devices such as liquid crystal displays (LCDs), and the tremendous increase in computing power. In its present form, integral imaging belongs to a broader class of multiview imaging systems that have been extensively researched for 3-D sensing, capture, and visualization of objects utilizing state-of-the-art optical and digital devices and techniques [1]. Compelling results have been demonstrated in applications such as display [12]–[15], automatic target recognition [16]–[21], [52], [55], target ranging [22], imaging in photon starved environments [23]–[28], imaging partially occluded or scattered objects [29]–[31], 3-D underwater imaging [32], [52], microscopy [18], [33], [34], and others [35]–[51], [53], [54], [56]–[64], [67]–[80] to name a few.

In this paper, we overview some of the recent advancements in the area of multiview passive imaging and their applications. The principles are reviewed in Section II. Several sensor configurations for optical pickup of 3-D images are discussed in Section III. Optical and computational display methodologies are covered in Section IV while several applications of 3-D sensing and display technologies have been presented in Section V. We conclude in Section VI with future directions and outlook. As is the case with any overview paper, it is not possible to present an exhaustive review of the field. Therefore, we may have inadvertently overlooked some relevant work, for which we apologize in advance.

II. PRINCIPLES OF INTEGRAL IMAGING

Integral imaging has a divide-and-conquer approach to the problem of 3-D sensing and display. This technique provides a window to the 3-D world through a collection of 2-D projections of real-world objects [6]. In this respect, the appealing features of integral imaging lies within its intimate connection with well-established and technologically mature 2-D image capture/display systems. In an integral imaging system, there are two separate procedures for acquisition and visualization of 3-D objects which are referred to as pickup and reconstruction stages, respectively.

In the pickup stage, multiple 2-D images (hereafter called elemental images) are captured through an array of small lenses (lenslet array). Each lenslet carries out a unique projective transformation that maps the 3-D object space onto 2-D elemental image and is a function of lenslet position and focal length [81]. Since each projective transform uniquely defines a perspective view, one can argue that each elemental image conveys a particular perspective of the objects in the scene. With such multipoint pickup configuration, both direction and intensity of rays emanating from the 3-D object can be recorded on the image sensor as depicted in Fig. 1(a). Note that each elemental image has its own unique perspective with respect to the scene. As a result, an array of inverted real images is formed on the image sensor each representing a unique 2-D projection of the 3-D object. To avoid crosstalk at the periphery of neighboring elemental images one can utilize parallax barriers on the image forming side of the lenslet array [13], [14].

For optical reconstruction of the scene, a 2-D LCD display projects the recorded integral image onto the focal plane of the display lenslet array with homogeneous (matched) pixel arrangement as of pickup lenslet array [see Fig. 1(b)]. Each elemental image is then optically relayed by its corresponding lenslet back into 3-D space. The overlap of all relayed elemental images creates local light distributions similar to the original object of interest. As a result, an observer can see a real 3-D image, albeit with inverted depth. This depth-reversed 3-D image is called a pseudoscopic real 3-D image because it is formed in front of the lenslet array on the observer side. To overcome this problem, pseudoscopic to orthoscopic conversion is required as depicted in Fig. 2. In essence, each elemental image is rotated by 180° around its center

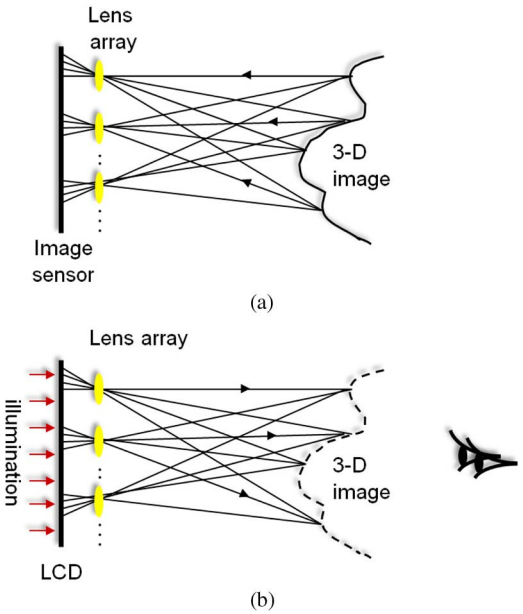

Fig. 1. *Principle of integral imaging. (a) Pickup. (b) Display.*

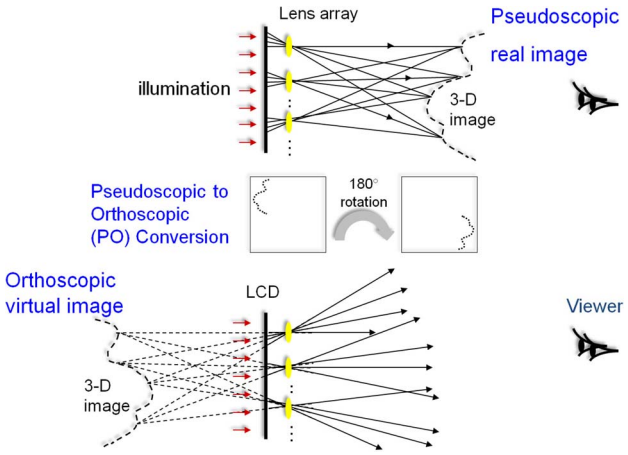

Fig. 2. ***Pseudoscopic-to-orthoscopic (P/O) conversion.***

point and the result is used to project onto the lenslet array as described before. In this way, orthoscopic (depth-corrected) virtual 3-D image of the objects is formed behind the lenslet array [13], [14], [68], [69]. The 3-D image formed in this way can be observed without the need for additional viewing glasses resulting in an autostereoscopic display which is highly desirable for next generation 3-D display technologies.

Although integral imaging can capture and visualize 3-D object using conventional 2-D imaging and display devices, there are important parameters that need to be considered including viewing resolution, viewing angle, and depth of focus. The viewing resolution can be defined by the resolution of the 3-D image which is observed from the viewing point. In an integral imaging system, parameters such as number of pixels and pixel size of the image sensor, lenslet pitch, and the number of lenslet affect the achievable viewing resolution [9], [11], [15], [35]. In an integral imaging system using a lenslet array, the total number of image sensor pixels is divided between elemental images. The number of pixels in each elemental image determines the achievable 3-D image viewing resolution. To improve the viewing resolution in an integral imaging system each lenslet can be replaced by a well-corrected, full frame imager [13].

The spatial frequency measured at the observation point can be used to describe the viewing resolution of an integral imaging system. Assuming that a single pixel per lenslet is observed, the Nyquist sampling theorem can be used to express the spatial frequency as [15], [35]

$$\beta_{\mathrm{Nyq}} \approx \frac{z_o}{2p} \tag{1}$$

in which β_{Nyq} is the spatial frequency in units of cycles per radian (cpr), p is the pitch of the lenslet array, and z_o is the distance between the observation point and the lenslet array as shown in Fig. 3. Note that reducing the parameter p to increase the viewing resolution is not always feasible, because diffraction of the small size lenslets degrades the resolution [9].

The viewing angle is limited to the field of view of each lenslet in which there is no crosstalk between adjacent lenslets (see Fig. 4) [36], [37]. If the observer moves out of the lenslet's field of view, each lenslet may relay the elemental image of its adjacent lenslet, resulting in appearance of an unwanted flipped image in the image space. Although parallax barriers can solve the display crosstalk problem, they put a hard limit on the viewing angle which can be defined mathematically as [37], [60]

$$\psi = 2\tan^{-1}\left(\frac{p}{2g}\right) \tag{2}$$

in which g is the distance between the lenslet array and the image sensor. The viewing angle can be improved by increasing lenslet pitch p and decreasing the focal length g. However, extended 3-D objects in the longitudinal direction may not be displayed clearly due to the short depth of focus associated with large size lenslets.

Fig. 5 illustrates that a point source can be reconstructed in the image space using an ideal diffraction-limited integral imaging system. For 3-D optical display, there are two types of ray integration [38], [39]. In the first type, which is called as resolution priority integral imaging (RPII), the distance between the display device and the lenslet array g should be larger than the focal length of each lenslet f as depicted in Fig. 5(a) and (b). Applying the Gauss

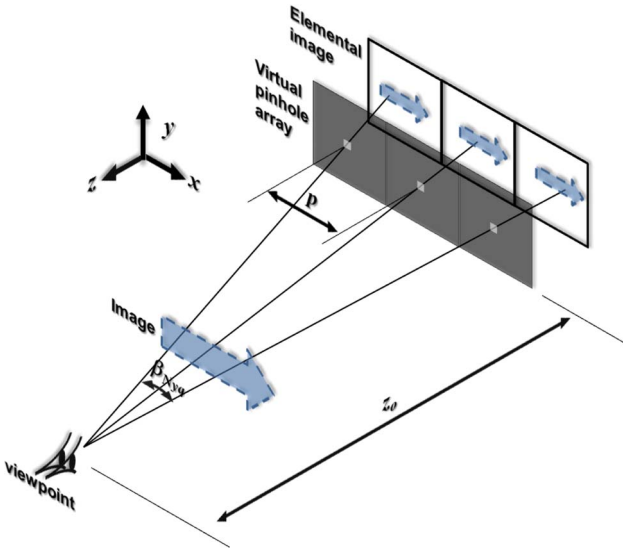

Fig. 3. ***Viewing resolution of integral imaging.***

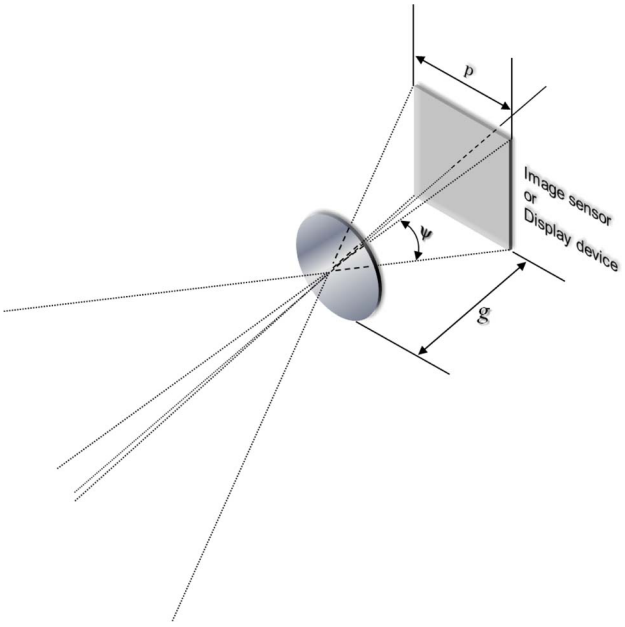

Fig. 4. *Viewing angle of integral imaging.*

lens law, the distance between the lenslet array and the lenslet image plane (LIP) is $z_o = gf/(g-f)$. Assuming square aperture lenslets, the maximum resolution R, in lines per millimeter in RPII mode can be found as [38], [39]

$$R = \frac{1}{a} = \frac{p}{2\lambda z_o} \tag{3}$$

in which $a = 2\lambda z_o/p$ is the spot size of reconstructed 3-D image and λ is the mean illumination wavelength, respectively.

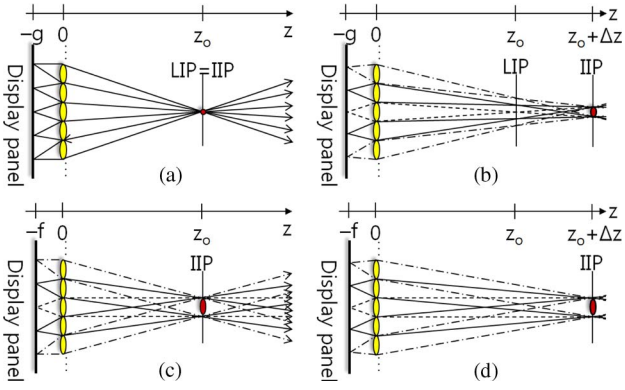

Fig. 5. *Two types of ray integration to produce 3-D images in integral imaging: (a) and (b) resolution priority integral imaging and (c) and (d) depth priority integral imaging.*

If the image sensor and the display device are located at the focal plane of the lenslet array ($g = f$), the system is known as depth priority integral imaging (DPII) as depicted in Fig. 5(c) and (d). In DPII, the LIP is far from the integral image plane (IIP) due to $z_o = \infty$. The rays from each lenslet propagate in parallel as plane waves. As a result, the spot size of each integral image pixel is equal to the lenslet size p. Therefore, the maximum resolution R in this mode can be written as

$$R = \frac{1}{a} = \frac{1}{p}. \tag{4}$$

Fig. 6(a) shows the imaging of point source by single lenslet. According to (3), when z_o is increased rapidly, the spot size of reconstructed point image is enlarged, i.e., R is decreased [see (3)]. Depth of focus (Δz_f) can be used as the depth limitation of the 3-D image. From the Fraunhofer diffraction theory [40], the diverging ray angle θ shown in Fig. 6(b) is given by $\theta = \sin^{-1}(\lambda/a) = \sin^{-1}(p/2z_o)$. Depth of focus is the distance between the focal point ($z = z_o$) and the position at minimum spot size when diffraction is taken into consideration. Now, since the 3-D image can be reconstructed both in the real and virtual fields, one can define the maximum depth of focus for an integral imaging system as [38]

$$D = 2\Delta z_f = 4\lambda z_o^2/p^2. \tag{5}$$

The 3-D image with a large depth can be reconstructed with DPII in which intercepting rays are less diverging than the case for RPII. The diverging ray angle θ is $\sin^{-1}(\lambda/p)$ as depicted in Fig. 6(c). Assuming that $\sin\theta \approx \tan\theta \approx \theta$, the maximum depth of focus for DPII can be calculated by

$$D = p^2/2\lambda. \tag{6}$$

III. SENSING STAGE OF INTEGRAL IMAGING

In traditional integral imaging pickup process, the quality of the acquired elemental images is a very important factor determining the 3-D image visualization quality. However, the tradeoffs present in the parameters of a lenslet-based integral imaging system make it difficult to achieve dense, high-resolution, large depth of field elemental image pickup. In what follows, various pickup schemes are described to mitigate these tradeoffs.

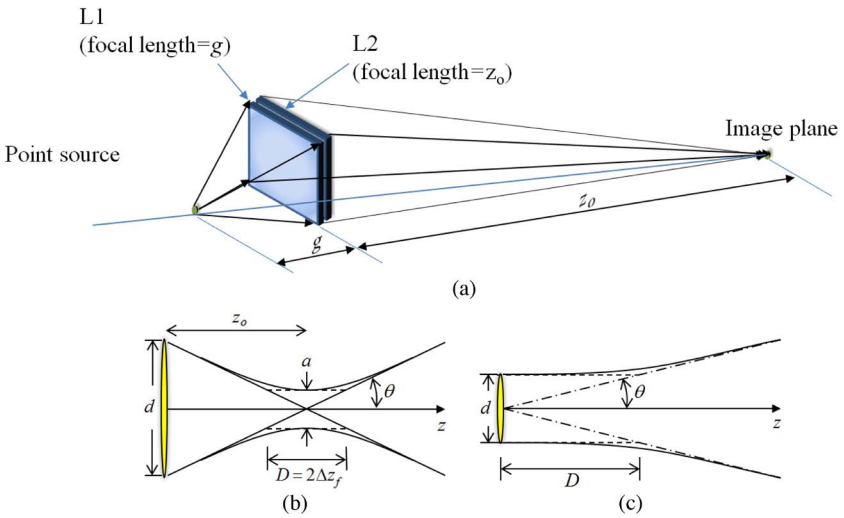

Fig. 6. *(a) Imaging of a point source by a single lenslet. Definition of 3-D image depth when (b)* $g > f$ *and (c)* $g = f$.

A. Direct Pickup

Fig. 7 illustrates the principle of direct pickup. One can record many elemental images with different perspectives directly by use of the lenslet array and a single image sensor. The 3-D image can then be observed by displaying the set of elemental images through the same lenslet array which results in a pseudoscopic real 3-D image. As described in Section II, the pseudoscopic 3-D image can be converted to a virtual othorscopic 3-D image by digitally rotating elemental images. However, the resolution of typical image sensors/displays are not sufficient for 3-D image capture or display, because the number of pixels allocated to each elemental image is reduced as the number of elemental images increases for a given sensor/display device. Several pickup methods have been proposed to enhance the quality of the 3-D image acquisition [41]–[43].

B. Electronically Synthesized Lenslets

An alternative way to using a molded lenslet array is to generate the array on an LCD device using Fresnel zone

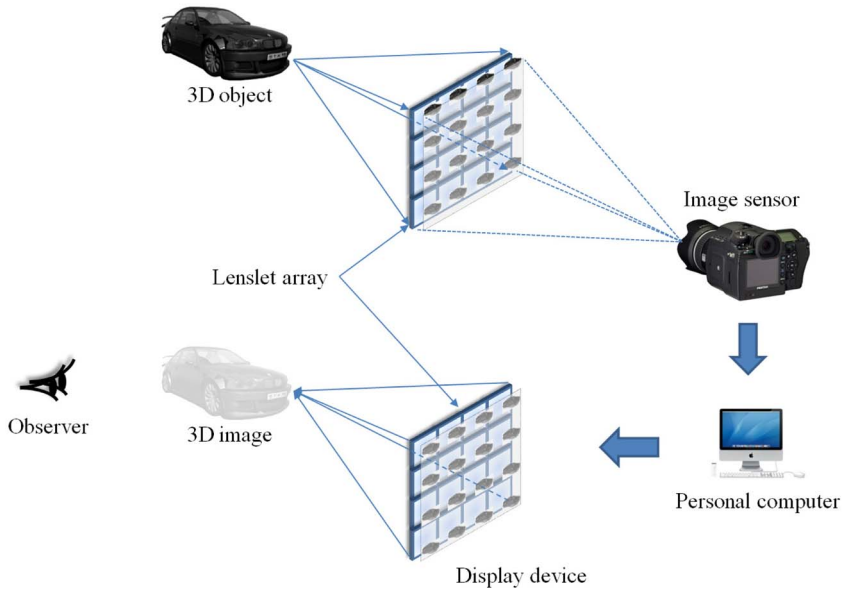

Fig. 7. *Principle of direct pickup and display for integral imaging.*

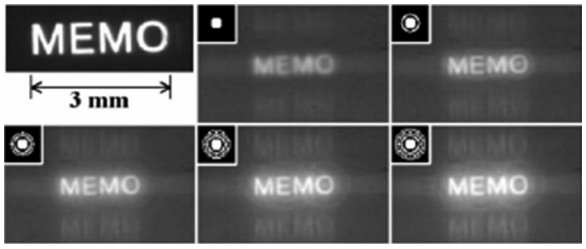

Fig. 8. *Images obtained with a Fresnel zone plate.*

plates in place of each lenslet [41]. The radius of the nth Fresnel zone r_n can be calculated by

$$r_n = (f_0 \lambda n + \lambda^2 n^2/4)^{1/2} \tag{7}$$

in which f_0 is the primary focal length. The advantage of electronically synthesized lenslet arrays is that the moving array lenslet technique (MALT) [35] can be implemented without mechanical motion. In MALT, multiple integral images are captured by moving the lenslet array in fractions of the lenslet pitch. This results in dense sampling of the ray space and therefore higher resolution of the resulting 3-D image.

Once multiple integral images are obtained, they can be projected on a lenslet array that moves synchronously with the elemental image set displayed using the projector. The mechanical motion has to be within the persistence time of human vision, i.e., ~40 ms, for the afterimage effect to result in perception of a high-resolution 3-D image. The elegance of electronically synthesized lenslet arrays is that no mechanical motion is required and the integral image displayed on the projector can be synchronized rapidly with the Fresnel zone plate array displayed on the LCD device.

Using Fresnel zone plates generated by (7), several images are obtained for $f_0 = 20$ mm and different numbers of zones as shown in Fig. 8.

C. Synthetic Aperture Integral Imaging (SAII)

One of the primary limitations of the lenslet-based integral imaging systems is the limited achievable resolution, in part due to the tradeoff between number of elemental images and number of pixels allocated to each elemental image. In essence, resolution of each elemental image is limited by three parameters: the pixel size, the lenslet point spread function, and the lenslet depth of focus. With a typical 1-mm pitch, plano-convex lenslets, only about 100 pixels (10 μm each) can be allocated to each elemental image. In addition, aberrations are significant and diffraction can adversely affect the elemental image resolution.

However, integral imaging can be performed either in a synthetic aperture mode or with an array of sensors in which an array of highly corrected lenses records each perspective image on a full size CCD or CMOS sensor of several megapixels [29], [42], [43]. Since the size of such an array quickly becomes a major concern, a single high-resolution 2-D imaging sensor can alternatively scan the aperture and capture intermittent images over a large area. This approach is known as synthetic aperture integral imaging (SAII) and overcomes some of the limitations of traditional lenslet-based integral imaging systems [29], [42], [43]. It should be noted that this method may not be suitable for dynamic scenes. Fig. 9 illustrates how the method can be implemented in practice.

D. Randomly Distributed Image Sensors

Integral imaging has been historically developed based on equally spaced, planar and regular grid of lenslets or lenticular elements. In the synthetic aperture regime, however, maintaining the same regularity might not be feasible for certain applications such as aerial 3-D imaging. In the process of collecting imagery across a large aperture, the position and orientation of sensors can hardly be restricted to what is prescribed by conventional pickup strategies, i.e., regular, planar grid. In [44], a method is suggested to relax some of the existing constraints on the pickup geometry. In particular, the position of pickup sensors can be randomly distributed in space as the synthetic aperture is being traversed by the sensor.

Affine transformation can be conveniently used to model the relationship between the object and image

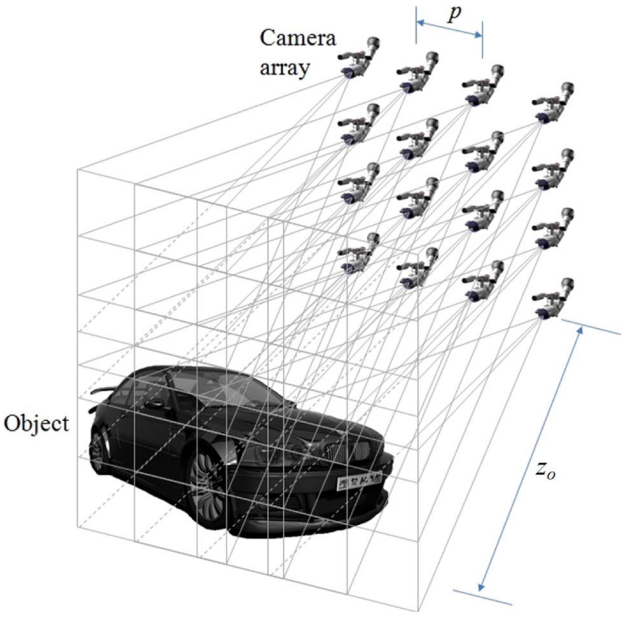

Fig. 9. *Synthetic aperture integral imaging (SAII).*

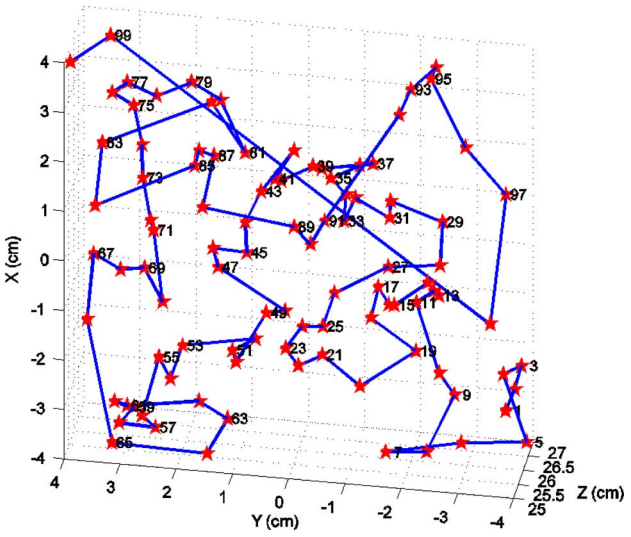

Fig. 10. ***Distribution of sensors within the pickup volume is random. Each red star denotes one of the 100 pickup positions.***

spaces for each sensor. If provided with relative position of randomly distributed sensors $(p^{x,y})$, this algorithm can reconstruct the object field from elemental images E_k for visualization or target recognition purposes as

$$R(x,y,z_r) \propto \sum_{k=0}^{K-1} E_k\left(\frac{x}{\gamma_k}+\frac{p_k^x-p_0^x}{M_k},\frac{y}{\gamma_k}+\frac{p_k^y-p_0^y}{M_k}\right) \quad (8)$$

where K is the total number of acquired image, M_k denotes the associated magnification of kth sensor relative to the desired reconstruction distance, and γ is the factor compensating for different magnification ratios of each sensor. In this form, the affine reconstruction equation requires constant computational and memory resources in contrast to distance-dependent backpropagation method. This feature translates into 2–3 orders of magnitude faster 3-D computational reconstruction speeds.

Fig. 10 shows the random distribution of 100 sensors in an area of $8 \times 8 \times 2$ cm^3 for imaging toy models of a tank and a sport car. Fig. 11 shows one of the sensor images along with reconstructions at distances 185 mm [Fig. 11(a)] and 240 mm [Fig. 11(b)].

E. Axially Distributed Image Sensors

While most multiview imaging systems are designed to capture different perspectives of real-world objects by sensors that are distributed laterally, i.e., perpendicular to the optical axis, ray space information can be recorded in an axially distributed scheme as well. In an axially distributed sensing (ADS) architecture [45], a single sensor is moved along its optical axis while recording intermittent images of the scene. In such an arrangement, the collection of 3-D information is not uniform across the sensor field of view. In fact, no parallax is available for points residing on the optical axis while parallax increases as objects get close to the periphery of the field of view. The angle subtended by the sensors with respect to an object point located at distance r from the optical axis and z_0 from the closest sensor can be written as

$$\Omega = \tan^{-1}\left(\frac{rs}{r^2+z_0^2+z_0 s}\right) \quad (9)$$

where s denotes the linear span of sensors along the optical axis as shown in Fig. 12. Equation (9) can be also used as a metric for 3-D information collection capacity of such a sensing scheme with respect to each object point. Note the special case of $r = 0$ where there is no parallax available, hence no 3-D information is obtained. The collected imagery can be reconstructed using the modified back-propagation technique taking into account the varying magnification ratio for each intermittent 2-D image [45].

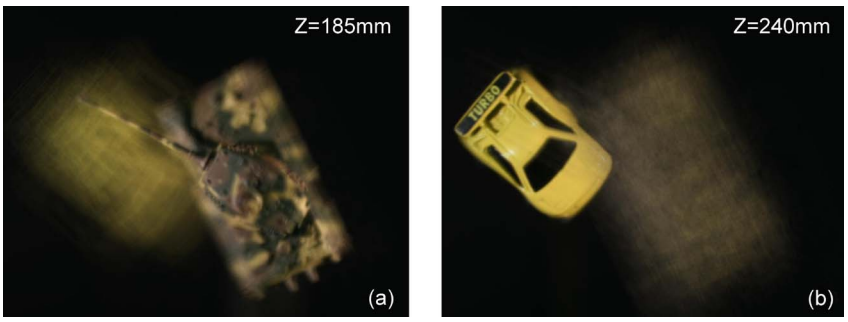

Fig. 11. ***Reconstruction of a scene containing two objects at (a) 185 mm and (b) 240 mm from the reference imager with randomly distributed sensors. The affine reconstruction equation takes into account and compensates for irregular pickup positions.***

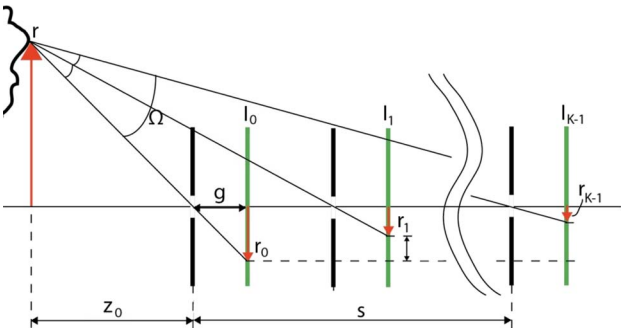

Fig. 12. *A single imager takes intermittent images as it moves along its optical axis in axially distributed sensing. The 3-D collection capability is nonuniform across the field of view and depends on the angle subtended by sensors from the object point.*

Fig. 13 shows reconstructed images of an object in front and behind a concentric ring occluding pattern. The center of the ring pattern coincides with the optical axis and hence is always in focus while 3-D information captured from objects in the periphery results in greater mismatch (hence blurring) at the reconstruction plane.

F. Multidimensional Optical Sensor and Imaging System (MOSIS)

Light and matter have a complex and intricate interaction and as a result, light reflected or emanated from an object is rich by information about the object. Often, conventional imaging systems only record a 2-D projection of the reflectivity of the object in the form of an intensity image. However, advanced image sensing systems can go beyond reflectivity information to record polarimetric, multispectral, or 3-D information by various techniques including time or space multiplexing. Fusion of the acquired imagery results in information rich representations of an object that can greatly improve object recognition performance.

One such system is the multidimensional optical sensor and imaging system (MOSIS) [46] in which various optical signatures are multiplexed for acquisition and fused to create a multidimensional image containing polarization, spectral, and reflectivity information of the object. The concept of MOSIS is illustrated in Fig. 14.

One can add 3-D information about the object by introducing integral imaging principles to such a system, in which case MALT can be used to increase the ray space sampling rate by time multiplexing resulting in improved resolution.

Also, polarization can open a new dimension in object's optical signatures. Typically, light reflected from dielectric and metallic surfaces exhibits different polarimetric information, which can be recorded by space-multiplexed polarization-sensitive detectors or by time multiplexing using Stokes polarimetry technique.

In low light conditions, nonvisual spectral bands can carry more information about the object. In particular, near-infrared (NIR) detectors can greatly improve imaging performance in such conditions. Sensitivity of conventional CCD detectors stretches into NIR band which can be properly exploited for hyperspectral sensing.

To merge the acquired multidimensional optical signatures from various imaging methods, multiresolution wavelet decomposition can be used [46]. Combining integral imaging, polarization, and multispectral imaging methods along with fusion algorithms using multiresolution wavelet decomposition is one way to realize a multidimensional optical imaging/display system.

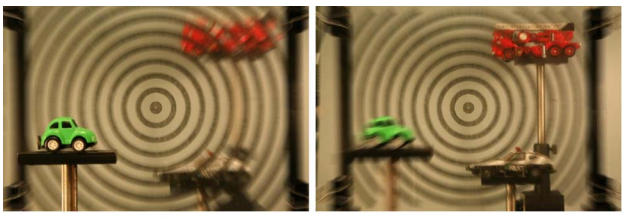

Fig. 13. *Computational plane-by-plane reconstruction with axially distributed sensing system at (a) 435 mm, where the green car is in focus, and (b) 805 mm, where the red fire truck is in focus.*

IV. VISUALIZATION USING INTEGRAL IMAGING

The information collected by an integral imaging system can be visualized three dimensionally using either optical displays or computational reconstruction methods. Optical displays provide full color, autostereoscopic images of an object with full parallax, and continuous viewing zones. However, low resolution of optical displays has limited their application. On the other hand, computational reconstruction methods have been developed to improve optical reconstruction by digital processing of acquired elemental images. Computational reconstruction provides a convenient way to reconstruct a high-quality 3-D image from an arbitrary perspective or to make planar reconstructions of the light field.

A. Optical Display

For optical display of integral images, a plano-convex lenslet array can be used. In essence, the reverse of optical pickup needs to be performed by the integral imaging display system. For this purpose, elemental images are projected onto the focal plane of the lenslet array using a 2-D display device. As a result, the object light field is reproduced in front (real pseudoscopic image) or behind (virtual orthoscopic image) the lenslet array as shown in Fig. 2. It is also possible to use gradient-index lenslet array for P/O conversion [14]. As the observation point changes, one can see different perspectives of the 3-D object. This is why integral imaging provides continuous viewing points. In such an optical

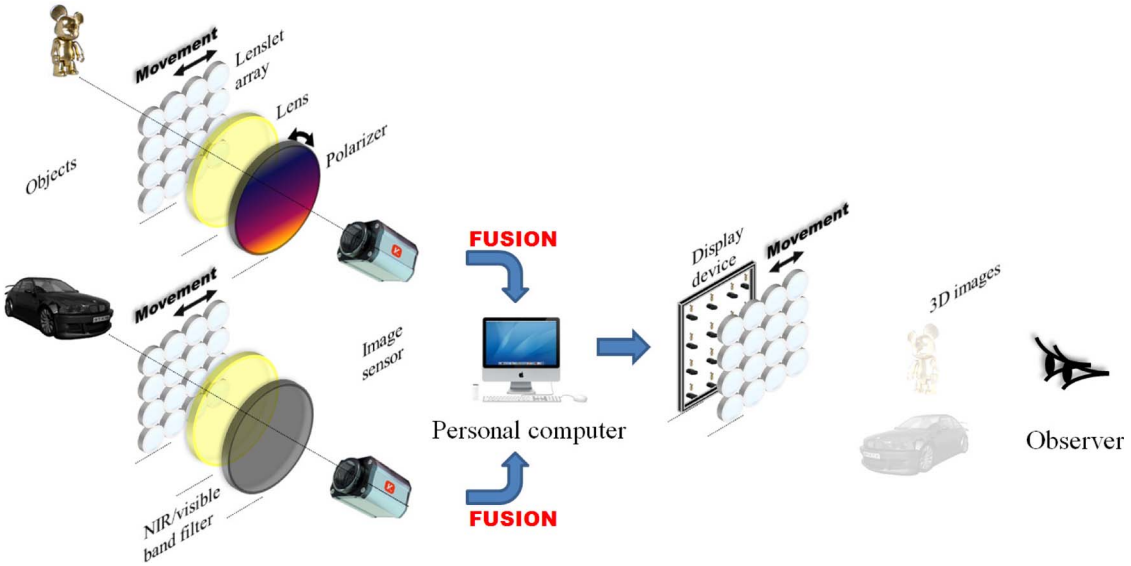

Fig. 14. ***Structure of multidimensional optical sensor and imaging system (MOSIS).***

display, the size of each elemental image should be the same as that of each lenslet. Also, the distance between the lenslet array and the display device should be approximately the same as that used in the pickup stage.

In projection integral imaging using lenslet array, the viewing resolution of the 3-D image can be improved [47], [54] by simultaneously using multiple image projectors as depicted in Fig. 15(a). However, the viewing angle is still limited because of the narrow field of view of each individual lenslet. To overcome these limitations, micromirror-array-based optical display has been suggested [47], [54]. In this technique, a micromirror array can be used in place of lenslet array to relay each projected elemental image into the image space and to create the 3-D image as shown in Fig. 15(b). Since micromirrors have small F-number, the viewing angle can be enhanced [see (2)]. Also, P/O conversion is not required anymore, because observers see only the reflected light from the projection screen. Therefore, orthoscopic virtual 3-D images can be automatically reconstructed, when the elemental images obtained from direct camera pickup are used.

The size of reconstructed 3-D image depends on the number and size of lenslets. Also, 3-D image quality can be determined by the number of pixels for each elemental image. Therefore, typically a large number of display lenslets and high-resolution elemental images are needed to reconstruct a large 3-D image with high quality. Spatio–temporally multiplexed projection integral imaging systems can deliver a better 3-D image quality comparing to conventional integral imaging displays. In spatial multiplexing, many display panels are used for the entire elemental image display as depicted in Fig. 15(a). Each display panel projects only a subset of entire elemental images onto the corresponding area of the projection screen. To reduce the number of display panels, temporal multiplexing between different panels can be implemented [48]. In this configuration, a single display panel projects multiple subsets of elemental images onto the corresponding area of the screen sequentially in time using galvanometer optical scanner as depicted in Fig. 16. The scanning time of all projections should be smaller than the persistence time of human vision for the flicker-free performance.

B. Computational Volumetric Reconstruction

Computational reconstruction of the 3-D image can be achieved by simulating the optical backprojection of elemental images in the computer (see, for example, [17], [29], [30], [43], and [53]). Using computational reconstruction methods, a physical phenomenon such as diffraction effects and device degradation can be avoided. Volumetric image reconstruction using elemental images is possible in the computer [17]. This reconstruction method uses a computer synthesized virtual pinhole array for inverse mapping of elemental images into the image space as illustrated in Fig. 17. In this method, each elemental image is projected on the desired reconstruction plane and is overlapped with all other backprojected elemental images. With this process, the light field can be reconstructed at arbitrary planes inside the 3-D object volume.

C. Profilometry and Optical Slicing

An ideal 3-D sensing system should be able to provide the coordinates of object points in 3-D space. Since multiview imaging systems rely on 2-D perspective images, the lateral coordinates (x, y) of objects are readily available. The third dimension, i.e., depth, has to be computed from the collected

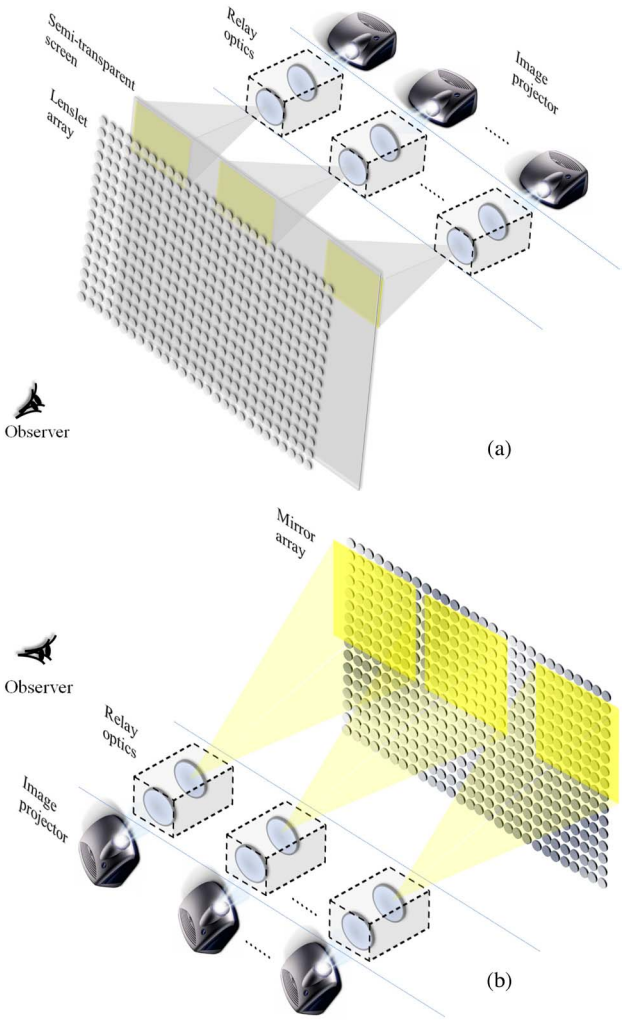

Fig. 15. ***(a) Projection-type integral imaging with lenslet array. (b) Projection-type integral imaging with microconvex mirror array.***

elemental images. For regular arrays of lenslets, the Fourier filter can be applied on the integral image to reduce the effect of out of focus [70]. In all its different forms, multiview imaging systems provide samples from a multidimensional function that characterizes different properties of a light ray in space. These properties can include angle, intensity, spectral content, and polarization. In [22], a convenient representation of such function is suggested as spectral radiation pattern (SRP) and a simple method is proposed for estimating object depth information based on images captured in a multiview system that includes integral imaging technique.

For each point in space (x, y, z), SRP parameterizes ray intensities based on their angle (θ, ϕ) and wavelength (λ) as

$$\Lambda(\theta, \phi, \lambda; x, y, z). \tag{10}$$

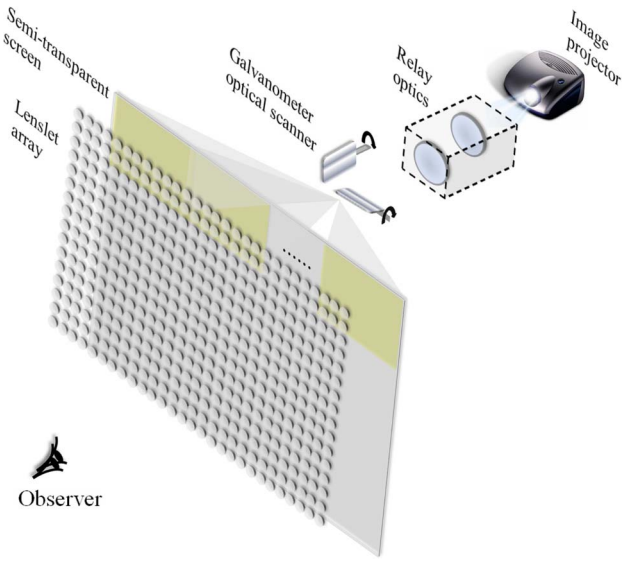

Fig. 16. ***System setup for integral imaging with spatio–temporal multiplexing.***

In practice, each pixel of an image in a multiview imaging system provides a single sample of the SRP along the associated chief ray. Therefore, for each point in space there is only one sample of SRP available in a 2-D image. Nevertheless, the number of samples increases with the number of sensors in a multiview imaging system. With more information available from the SRP at each point in space, one can estimate the depth of object points using statistical methods [22].

Note that the difference between an object point and a free-space point is revealed in their respective SRP (see Fig. 18). The samples of the SRP of a Lambertian object point are expected to have a small variation, whereas a free-space point is the crossing of different rays coming

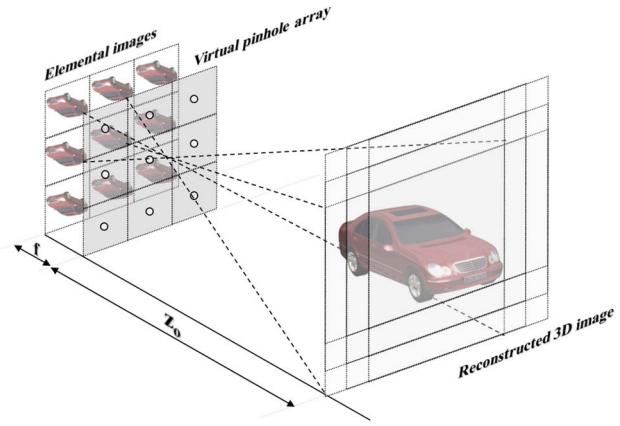

Fig. 17. ***Computational volumetric reconstruction.***

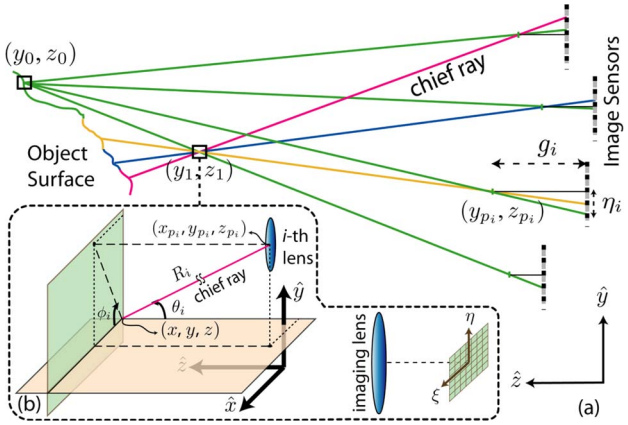

Fig. 18. *(a) Ray diagram showing SRP of object versus free space point. The variation of SRP for free space points is used to estimate the depth of object points. (b) Single imager sampling the SRP at point* (x, y, z)*.*

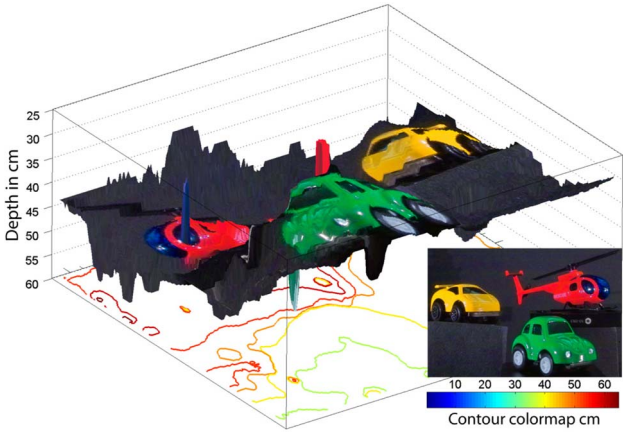

Fig. 19. *Estimated depth information with passive profilometry based on 121 perspective images. Inset shows the original scene.*

from different parts of the object, hence exhibit larger variation. This variation can be used to estimate the depth of each point as

$$\hat{z}(x,y) = \arg\max_{z \in Z} \left[\Lambda(\theta, \phi, \lambda) - \overline{\Lambda}\right]^2 \qquad (11)$$

where $\overline{\Lambda}$ denotes the mean of the SRP over all parameters and Z signifies the range of objects of interest. Once the depth of object points is recovered, one can extract sectional images of the scene similar to the laser radar. However, unlike laser radar, multiview-imaging-based profilometry is passive and provides texture and spectral information as well as depth information.

Fig. 19 illustrates the recovered depth information from an ensemble of 121 elemental images based on (11). The misestimated points are due to the specular reflection from the surface of the objects which departs from the Lambertian assumption.

V. APPLICATIONS OF 3-D SENSING AND DISPLAY

In this section, several applications of 3-D integral imaging system are presented. In each case, the advantages of 3-D sensing using integral imaging enables new capabilities or improves the performance in the described application.

A. Underwater Imaging

For imaging in aquatic environments, numerous effects like wavelength-dependent absorption, scattering, dispersion, and index of refraction variations should be considered. At the interface between air and water, the rays are refracted from the straight propagation direction according to Snell's law. As a result, objects underwater appear floating to the in-air observer. For imaging perpendicular to air–water interface, the object distance z_{water} should be adjusted according to the water refractive index, i.e., $z'_{\text{water}} = z_{\text{water}}/n_{\text{water}}$ [32], [53] where z_{water} is the actual distance between water surface and objects, n_{water} is the refraction index of water, and z'_{water} is the reconstruction distance between the water surface and objects as depicted in Fig. 20. This results in a shorter reconstruction distance in comparison to the actual distance between image sensors and underwater objects. Fig. 21 illustrates objects used in underwater imaging and 3-D reconstruction results. Considering the geometrical alteration due to the difference in refraction index of water (≈1.33) and air (≈1.00), the volumetric 3-D underwater images can be reconstructed as shown in Fig. 21(c)–(f).

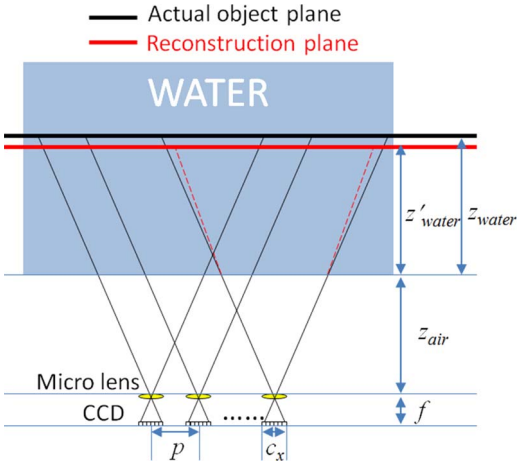

Fig. 20. *3-D reconstruction of underwater objects using integral imaging.*

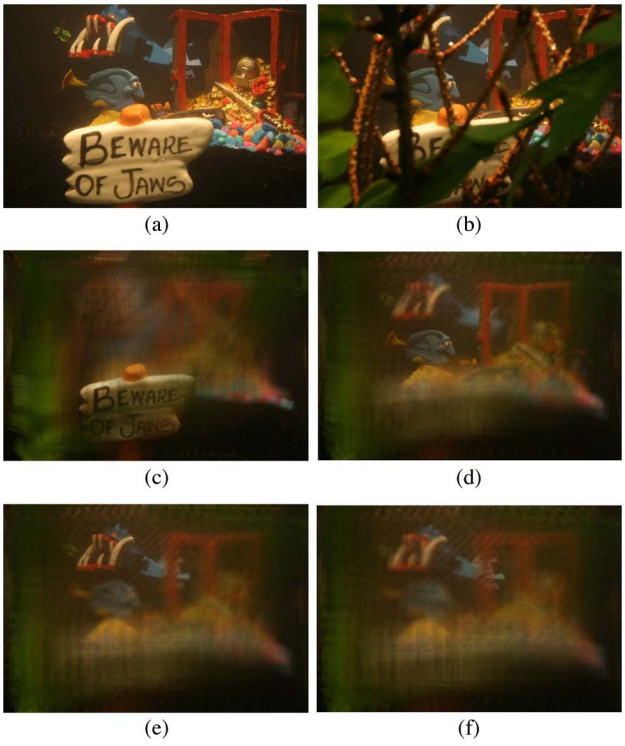

Fig. 21. *Experimental results for underwater imaging. (a) A central 2-D perspective image of the unoccluded in-water scene. (b) The same 2-D perspective image as (a) with heavy foreground occlusion. (c)–(f) 3-D computational reconstruction at $z = 230$ mm, $z = 380$ mm, $z = 440$ mm, and $z = 480$ mm.*

B. Passive Near-Infrared Integral Imaging

In low light environments, the image of the desired object cannot be detected appropriately using conventional visible spectrum imaging systems. Imaging in nonvisible spectral bands can alleviate this problem; however, this signal is often weak or may not reach the detector due to occlusion. Using integral imaging, low NIR signals from each perspective can be put together by computational reconstruction to visualize the object of interest in 3-D [49]. Fig. 22 is the schematic diagram of passive NIR imaging system using integral imaging. Such imaging system has the advantage of reducing the effect of occlusion due to multiple perspectives available by integral imaging pickup. Fig. 23 shows the reconstruction results of passive NIR imaging system.

C. Photon-Counting Image Visualization (Poisson and Truncated Poisson Models With Maximum-Likelihood Estimate)

Integral imaging technique is potentially useful for visualization of objects in extremely dark environments. For 3-D sensing of a photon-limited object, the 3-D integral imaging utilizes a camera array in order to record the low intensity level light ray emanating from 3-D object. Each one of the camera array captures its own photon-counted 2-D elemental image, which contains directional information of the 3-D object. Then, 3-D reconstruction of the original object can be digitally performed by applying computational ray backpropagation algorithm and parametric maximum-likelihood estimator (MLE) to the acquired photon-counted elemental images [23]–[28]. In this way, the irradiance of one voxel of photon-limited 3-D object is recorded on the corresponding pixel position of each photon-limited 2-D elemental image. The recorded pixel values for the one voxel of the photon-limited 3-D object are assumed to be a random variable following the *Poisson* distribution function. Each voxel value of the original 3-D object can be retrieved by applying the parametric MLE to the pixel values as follows [26], [28]:

$$\begin{aligned}\mathrm{MLE}(\tilde{N}I_v) &= \arg\max_{\tilde{N}I_v}\left[\log\prod_{n=1}^{N_e}\exp(-\tilde{N}I_v)(\tilde{N}I_v)^{c_v(n)}\right] \\ &= \frac{1}{N_e}\sum_{n=1}^{N_e}c_v(n) \qquad (12)\end{aligned}$$

where C_v is the *Poisson* random number with the mean parameter $\tilde{N}I_v$ at each voxel of the reconstructed image, where subscript v denotes a voxel index, $\tilde{N}$ is the expected number of photons in the photon-limited elemental image, I_v is the normalized irradiance, and N_e is the total number of elemental images [26].

Since the dispersion of *Poisson* distribution possibly overestimates or underestimates the variance of the observed samples in case that a small number of photons is available, the single rate parameter of *Poisson* distribution might not be

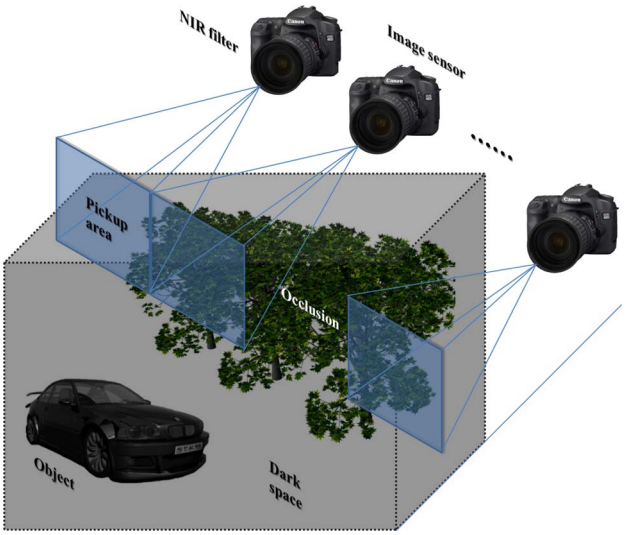

Fig. 22. *NIR imaging system.*

Fig. 23. *NIR experimental results: (a) unoccluded heated soldering iron in NIR range, (b) occluded soldering iron in NIR range without external illumination, and (c) occluded heated soldering iron in visible range with external illumination.*

enough to represent the population. Therefore, a truncated *Poisson* density function can be replaced for better modeling of the distribution of the photo-count observations.

Similarly, each voxel value for 3-D object is estimated by applying computational ray backpropagation algorithm and MLE on the truncated *Poisson* distribution for 3-D imaging of an object in extremely dark environment. It is demonstrated that the estimated value for one voxel value of 3-D object using a truncated *Poisson* model has small estimation error compared with the MLE using a *Poisson* model [27].

Fig. 24 shows the rear and front views of a toy car. Fig. 25 shows the sectional images of the rear and front views reconstructed from a very small number of photon-counted elemental image set by using the truncated photon-counting model.

D. 3-D Integral Imaging in Scattering Medium

Integral imaging can be performed with coherent illumination for various spectral specific applications. In this case, it can recover 3-D object information embedded in a scattering media as shown in Fig. 26 [31]. In this method, the scattered elemental image set for the objects in the scattering media is recorded by using integral imaging under coherent illumination. The elemental image set contains the interference patterns between scattered and original object beams, which have the form similar to a phase-modulated function [31]. The interference term can be regarded as a random variable with zero mean because of many scattered beams with different phases.

Since integral imaging provides multiple independent measurements with a camera array, the elemental images of the scattered object at the pth pixel position corresponding to each voxel of the original 3-D object can be described as follows [31]:

$$I_p^s(i) = I_p^o + w_p(i), \qquad \text{for } i = 1, \ldots, N \tag{13}$$

where $I_p^s(i)$ and $I_p^o(i)$ are scattered and original object beam intensities, respectively, and $w_p(i)$ is a random variable following an independent and identically distributed statistical model.

For 3-D imaging for scattered objects, the computational ray backpropagation algorithm is applied to the scattered elemental image set in order to eliminate or average out the distortion term $(w_p(i))$ in (13).

Fig. 27 shows the first nonscattered and scattered elemental images, respectively. Fig. 28 show the sectional images reconstructed at different distances from the scattered elemental image sets by using the integral imaging technique.

E. 3-D Tracking of Objects in Occlusion

The computational volumetric reconstruction using integral imaging can reduce the occlusion by refocusing the light field at the desired object distance. As a result,

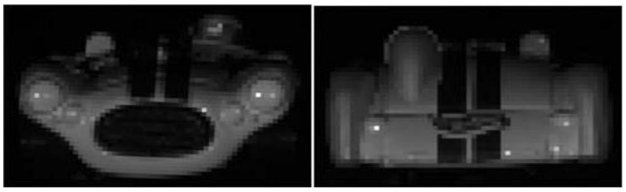

Fig. 24. *Toy car used in the experiments. (a) Front view. (b) Rear view.*

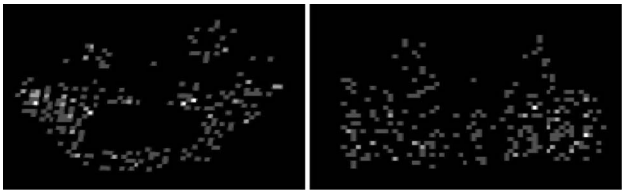

Fig. 25. *Sectional images of toy cars reconstructed from a very small number of photon-counted elemental images set by using the truncated photon-counting model. The total number of the elemental images was 25. (a) Reconstructed front view car. (b) Reconstructed rear view car.*

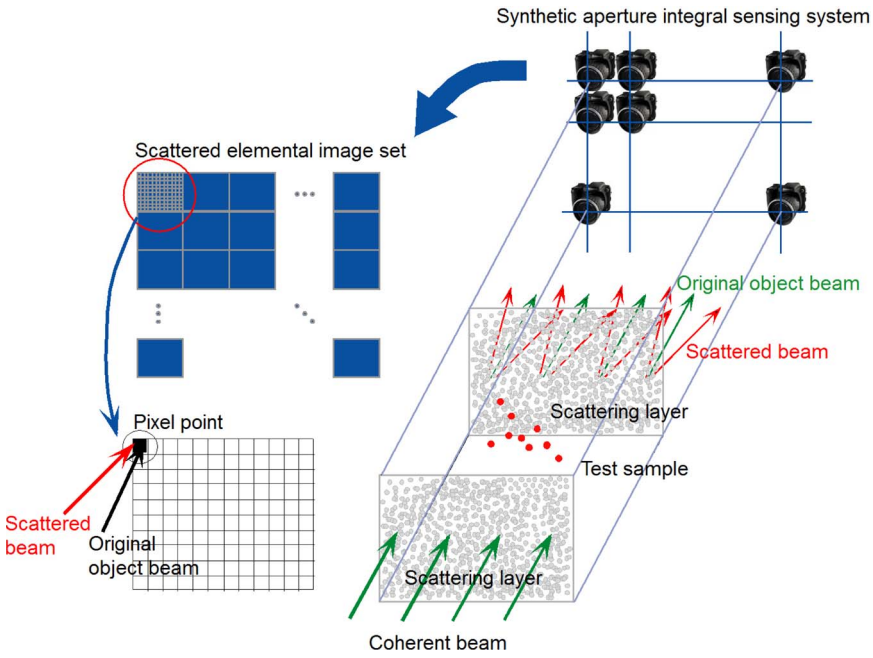

Fig. 26. *A schematic setup of a coherent integral imaging system for 3-D imaging of scattered objects.*

moving objects behind heavy occlusion can be tracked using integral imaging [50]. A simple tracking algorithm known as "summation of absolute difference (SAD)" is a block-based correspondence algorithm [65], useful for object tracking. It computes the intensity differences for each pixel in a target window t_x by t_y as follows:

$$\mathrm{SAD}(x,y) = \sum_{p=0}^{t_x-1}\sum_{q=0}^{t_y-1}|R_n(x+p,y+q) - T_{n-1}(p,q)| \quad (14)$$

where $R_n(\cdot)$ is the nth frame reconstructed 3-D image, $T_{n-1}(\cdot)$ is the target pixel matrix which is obtained from $(n-1)$th frame reconstructed 3-D image, and r_x, r_y are the number of pixels for each frame image in the x- and y-directions. To enhance the tracking quality, the absolute of edge values is used instead of the pixel value.

Fig. 29 represents the 3-D moving path of the occluded object. The 3-D path is random to verify that this tracking method can implement object tracking in 3-D. Fig. 30 shows some sequence images of the tracking result. The occluded object is tracked by using the edge-value-based SAD algorithm.

F. 3-D Microscopy Using Integral Imaging for Visualization and Identification of Cells

Integral imaging has been considered for microscopy [33], [34], [82], [83] and identification of biological micro-organisms [18]. In the 3-D visualization of micro-objects,

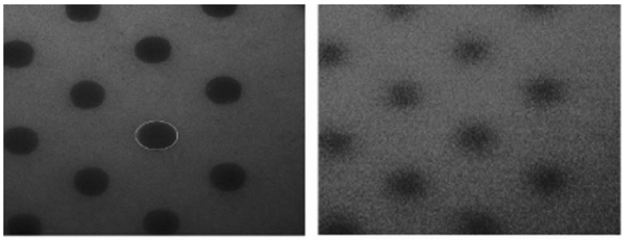

Fig. 27. *(a) Nonscattered and (b) scattered images.*

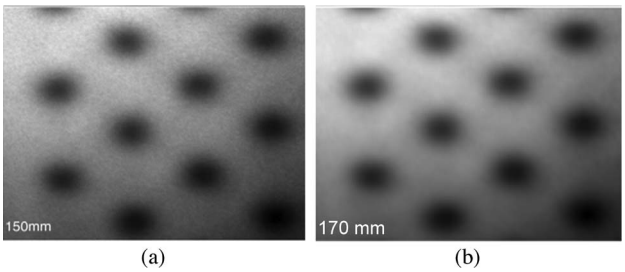

Fig. 28. *The sectional images reconstructed at different distances from the scattered elemental image sets by using integral imaging. (a) 150 mm. (b) 170 mm.*

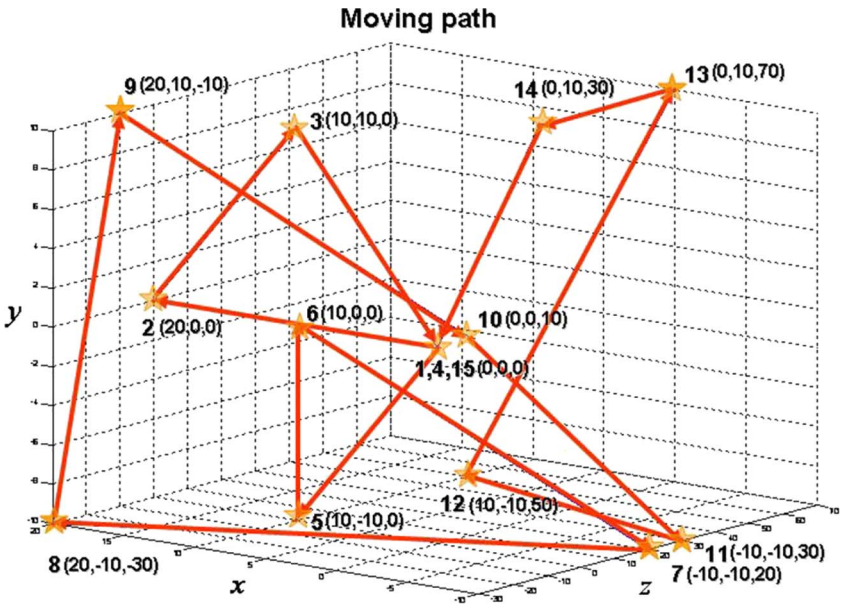

Fig. 29. ***3-D moving path of the occluded object.***

the use of magnifying lenses before the pickup process may cause a problem because of the nonuniform longitudinal magnification. To reconstruct 3-D images of micro-objects, uniformly magnified 2-D elemental images are required. Confocal microscopy [66] can generate uniformly magnified sectional images of 3-D micro-objects for a different depth (z).

The light intensity distributions of the kth sectional image for the ith virtual pinhole is given by $V_C(x_i, y_i, z = z_k)$, where subscript $C = 1$ (for red), 2 (for green), and 3 (for blue), and the light intensity distribution of the corresponding pickup surface $S_C(x_i, y_i, z = -g)$ becomes [33]

$$S_C(x_i, y_i, -g) = \sum_{k=1}^{N} A_C(k) V_C(x_i, y_i, z_k) \tag{15}$$

$$A_C(k) = \begin{cases} e^{-\alpha k}, & \text{if } V_C \neq 0 \\ 1, & \text{otherwise} \end{cases} \tag{16}$$

where x_i and y_i are the local coordinates for the ith virtual pinhole, $A_C(k)$ is the light absorption of the kth sectioning image, N is the number of sectioning images, and α is the light absorption coefficient (e.g., $\alpha = 0.05$).

Using (15) and (16), computer synthesized elemental images can be obtained as depicted in Fig. 31. Fig. 32(a) shows optical experimental results at three viewing points (left, front, and right view). The low quality of reconstructed 3-D images is the result of low-resolution elemental images and can be mitigated by using the MALT technique described in Section III-B. Fig. 32(b) shows the reconstruction results using MALT [35], [82], which exhibit better visual quality. However, the high spatial frequencies are compromised because of the afterimage effect.

Recently, digital holographic microscopy has been proposed for identification of micro/nanoorganisms, cells, etc. [84], [85]. In addition, integral imaging has been proposed for cell identification [18]. Fig. 33 illustrates the 3-D sensing and visualization of the microorganisms using integral imaging microscopy. The 3-D reconstructed images of the cells and/or microorganisms can be processed by statistical pattern recognition for identification and classification.

VI. CONCLUSION

The resurrection of integral imaging principles from the early twentieth century in the past decade has created a dynamic and fast paced field for research and application development in the area of 3-D sensing and display. Remarkable improvements in commercially available optoelectronic sensor and displays as well as exponential increase in access to inexpensive computational power have fueled the progress in the field of multiview 3-D imaging. The elegance of multiview-based imaging and display systems lies in their simplicity and scalability and their reliance on mature 2-D imaging/display devices. Systems of this sort are typically less complex and costly than their holographic counterparts, which require coherent illumination, are plagued by speckle noise, and have limitations in outdoor scenes.

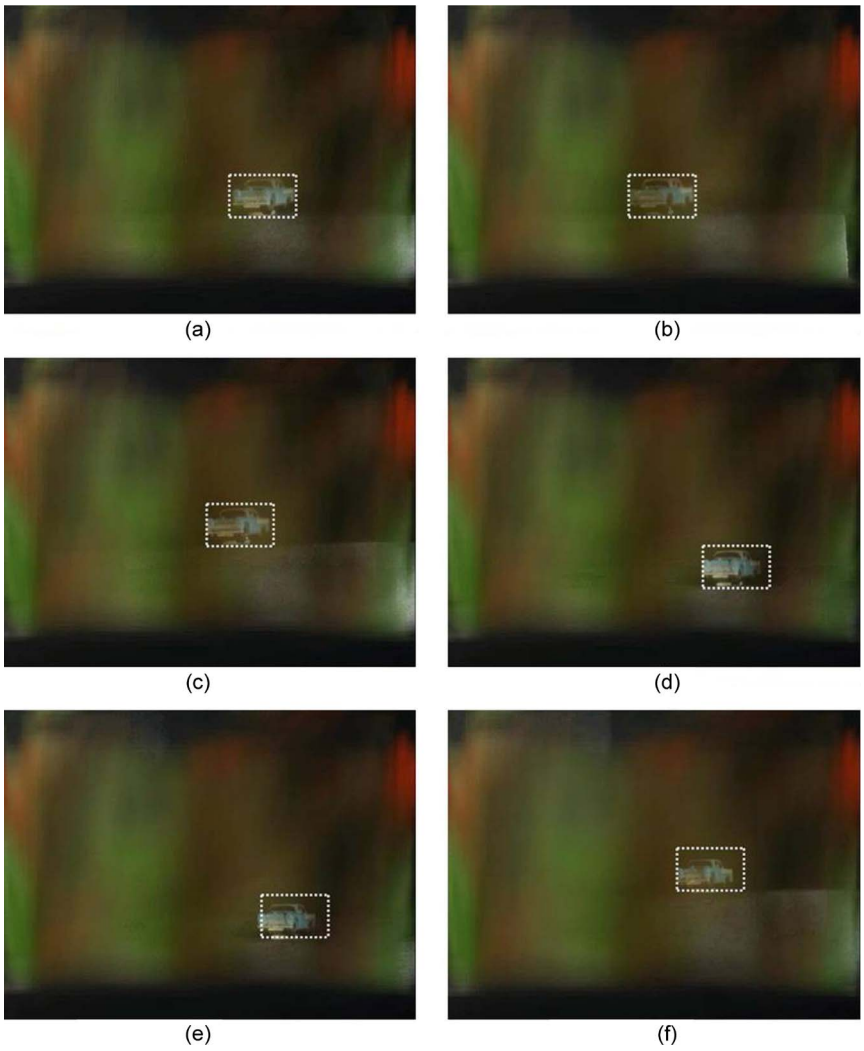

Fig. 30. *3-D tracking results: (a) first frame, (b) second frame, (c) third frame, (d) seven frame, (e) eleventh frame, and (f) thirteenth frame.*

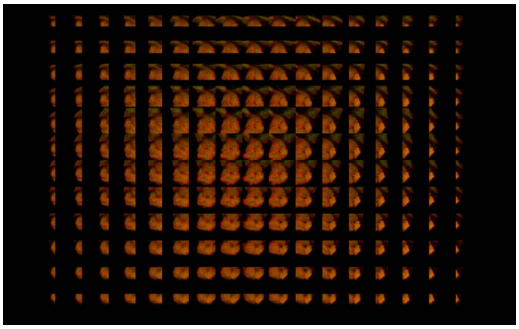

Fig. 31. *Computer synthesized elemental images of the 3-D micro-object.*

These characteristics make passive sensing multiview imaging systems ready to be deployed in various applications in large scales. Already, passive 3-D displays are finding their way into commercial 3-D TV industry. Also, multiview imaging systems are proven to shift the paradigm in sensing and processing strategies in a number of fields including medical imaging, defense and security as well as industrial manufacturing. In the meantime, fundamental research in this area continues to generate fruitful results.

The advancements in detector arrays with small pixel size and development of alternatives to lens-based imaging can take multiview sensing to a new level in which the light field can potentially be sampled with very high resolution. Computational–optical sensing methods can in

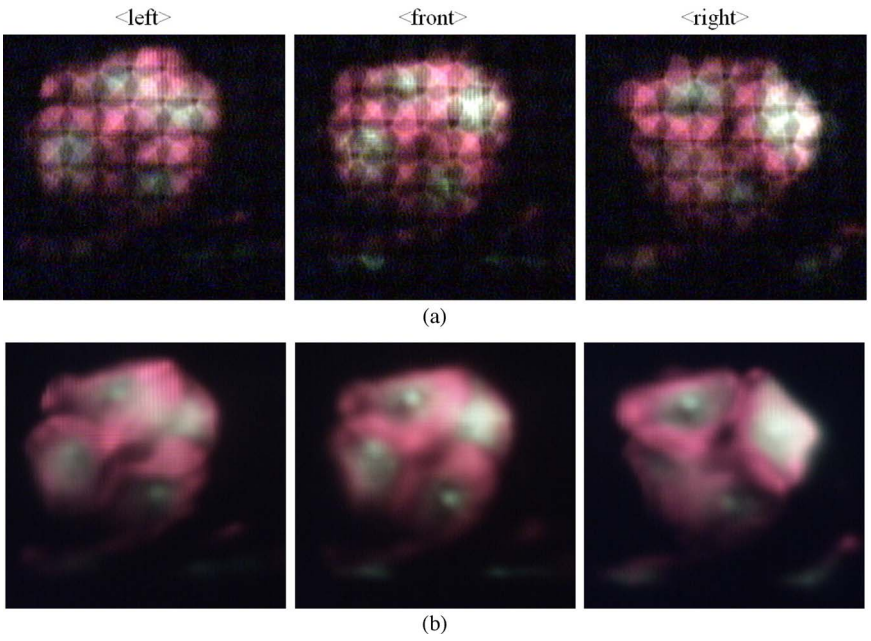

Fig. 32. ***Optical experimental results using (a) conventional integral imaging and (b) MALT.***

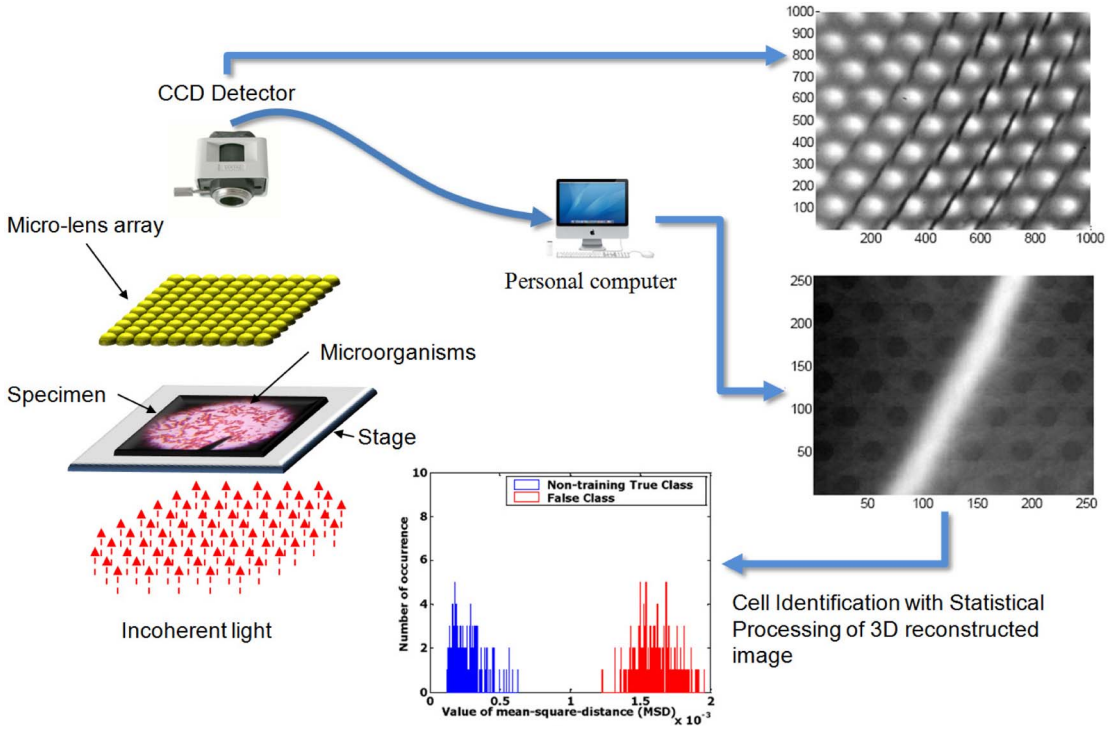

Fig. 33. ***Cell identification with 3-D integral imaging.***

principle be jointly designed and optimized to replace direct pickup structure in order to decode, augment, or otherwise enhance the information being displayed. In summary, multiview 3-D sensing and display is an enabling technology and new applications are yet to be discovered in the years ahead. ■

REFERENCES

[1] B. Javidi, F. Okano, and J.-Y. Son, *Three-Dimensional Imaging, Visualization, and Display Technology*. New York: Springer-Verlag, 2008.

[2] S. A. Benton and V. M. Bove, *Holographic Imaging*. New York: Wiley-Interscience, 2008.

[3] A. Stern and B. Javidi, "Three-dimensional image sensing, visualization, and processing using integral imaging," *Proc. IEEE*, vol. 94, no. 3, pp. 591–607, Mar. 2006.

[4] C. Wheatstone, "On some remarkable, and hitherto unobserved, phenomena of binocular vision," *Phil. Trans. R. Soc. London*, vol. 128, pp. 371–394, 1838.

[5] L. Lypton, *Foundation of Stereoscopic Cinema*. New York: Van Nostrand Reinhold, 1982.

[6] G. Lippmann, "La Photographie Integrale," *Comptes-Rendus Academie des Sciences*, vol. 146, pp. 446–451, 1908.

[7] A. P. Sokolov, *Autostereoscopy and Integral Photography by Professor Lippmann's Method*. Moscow, Russia: Moscow State Univ. Press, 1911.

[8] H. E. Ives, "Optical properties of a lippmann lenticuled sheet," *J. Opt. Soc. Amer.*, vol. 21, pp. 171–176, 1931.

[9] C. B. Burckhardt, "Optimum parameters and resolution limitation of integral photography," *J. Opt. Soc. Amer.*, vol. 58, pp. 71–76, 1968.

[10] T. Okoshi, *Three-Dimensional Imaging Techniques*. New York: Academic, 1976.

[11] T. Okoshi, "Three-dimensional displays," *Proc. IEEE*, vol. 68, no. 5, pp. 548–564, May 1980.

[12] L. Yang, M. McCornick, and N. Davies, "Discussion of the optics of a new 3-D imaging system," *Appl. Opt.*, vol. 27, pp. 4529–4534, 1988.

[13] F. Okano, J. Arai, K. Mitani, and M. Okui, "Real-time integral imaging based on extremely high resolution video system," *Proc. IEEE*, vol. 94, no. 3, pp. 490–501, Mar. 2006.

[14] J. Arai, F. Okano, H. Hoshino, and I. Yuyama, "Gradient index lens array method based on real time integral photography for three dimensional images," *Appl. Opt.*, vol. 37, pp. 2034–2045, 1998.

[15] H. Hoshino, F. Okano, H. Isono, and I. Yuyama, "Analysis of resolution limitation of integral photography," *J. Opt. Soc. Amer. A*, vol. 15, pp. 2059–2065, 1998.

[16] O. Matoba, E. Tajahuerce, and B. Javidi, "Real-time three-dimensional object recognition with multiple perspectives imaging," *Appl. Opt.*, vol. 40, pp. 3318–3325, 2001.

[17] S.-H. Hong, J.-S. Jang, and B. Javidi, "Three-dimensional volumetric object reconstruction using computational integral imaging," *Opt. Exp.*, vol. 12, pp. 483–491, 2004.

[18] B. Javidi, I. Moon, and S. Yeom, "Three-dimensional identification of biological microorganism using integral imaging," *Opt. Exp.*, vol. 14, pp. 12 095–12 107, 2006.

[19] Y. Frauel and B. Javidi, "Digital three-dimensional image correlation using computer-reconstructed integral imaging," *Appl. Opt.*, vol. 41, pp. 5488–5496, 2002.

[20] S. Kishk and B. Javidi, "Improved resolution 3-D object sensing and recognition using time multiplexed computational integral imaging," *Opt. Exp.*, vol. 11, pp. 3528–3541, 2003.

[21] S.-H. Hong and B. Javidi, "Distortion-tolerant 3D recognition of occluded objects using computational integral imaging," *Opt. Exp.*, vol. 14, pp. 12 085–12 095, 2006.

[22] M. Daneshpanah and B. Javidi, "Profilometry and optical slicing by passive three-dimensional imaging," *Opt. Lett.*, vol. 34, pp. 1105–1107, 2009.

[23] S. Yeom, B. Javidi, and E. Watson, "Photon counting passive 3D image sensing for automatic target recognition," *Opt. Exp.*, vol. 13, pp. 9310–9330, 2005.

[24] S. Yeom, B. Javidi, C.-W. Lee, and E. Watson, "Photon-counting passive 3D image sensing for reconstruction and recognition of partially occluded objects," *Opt. Exp.*, vol. 15, pp. 16 189–16 195, 2007.

[25] S. Yeom, B. Javidi, and E. Watson, "Three-dimensional distortion-tolerant object recognition using photon-counting integral imaging," *Opt. Exp.*, vol. 15, pp. 1513–1533, 2007.

[26] B. Tavakoli, B. Javidi, and E. Watson, "Three dimensional visualization by photon counting computational integral imaging," *Opt. Exp.*, vol. 16, pp. 4426–4436, 2008.

[27] I. Moon and B. Javidi, "Three dimensional imaging and recognition using truncated photon counting model and parametric maximum likelihood estimator," *Opt. Exp.*, vol. 17, pp. 15 709–15 715, 2009.

[28] I. Moon and B. Javidi, "Three-dimensional recognition of photon-starved events using computational integral imaging and statistical sampling," *Opt. Lett.*, vol. 34, pp. 731–733, 2009.

[29] S.-H. Hong and B. Javidi, "Three-dimensional visualization of partially occluded objects using integral imaging," *IEEE/OSA J. Display Technol.*, vol. 1, no. 2, pp. 354–359, Dec. 2005.

[30] V. Vaish, M. Levoy, R. Szeliski, C. L. Zitnick, and S. B. Kang, "Reconstructing occluded surfaces using synthetic apertures: Stereo, focus and robust measures," in *Proc. IEEE Comput. Soc. Conf. Comput. Vis. Pattern Recognit.*, 2006, vol. 2, pp. 2331–2338.

[31] I. Moon and B. Javidi, "Three-dimensional visualization of objects in scattering medium by use of computational integral imaging," *Opt. Exp.*, vol. 16, pp. 13 080–13 089, 2008.

[32] R. Schulein and B. Javidi, "Underwater multiview three-dimensional imaging," *IEEE/OSA J. Display Technol*, vol. 4, no. 4, pp. 351–353, Dec. 2008.

[33] J.-S. Jang and B. Javidi, "Three-dimensional integral imaging of micro-objects," *Opt. Lett.*, vol. 29, pp. 1230–1232, 2004.

[34] M. Levoy, Z. Zhang, and I. McDowall, "Recording and controlling the 4D light field in a microscope using microlens arrays," *J. Microscopy*, vol. 235, pp. 144–162, 2009.

[35] J.-S. Jang and B. Javidi, "Improved viewing resolution of three-dimensional integral imaging by use of nonstationary micro-optics," *Opt. Lett.*, vol. 27, pp. 324–326, 2002.

[36] F. Okano, H. Hoshino, J. Arai, and I. Yuyama, "Three-dimensional video system based on integral photography," *Opt. Eng.*, vol. 38, pp. 1072–1077, 1999.

[37] J.-S. Jang and B. Javidi, "Improvement of viewing angle in integral imaging by use of moving lenslet arrays with low fill factor," *Appl. Opt.*, vol. 42, pp. 1996–2002, 2003.

[38] J.-S. Jang, F. Jin, and B. Javidi, "Three-dimensional integral imaging with large depth of focus by use of real and virtual image fields," *Opt. Lett.*, vol. 28, pp. 1421–1423, 2003.

[39] J.-S. Jang and B. Javidi, "Large depth-of-focus time-multiplexed three-dimensional integral imaging by use of lenslets with nonuniform focal lengths and aperture sizes," *Opt. Lett.*, vol. 28, pp. 1924–1926, 2003.

[40] J. W. Goodman, *Introduction to Fourier Optics*. New York: McGraw-Hill, 1996.

[41] J.-S. Jang and B. Javidi, "Three-dimensional integral imaging with electronically synthesized lenslet array," *Opt. Lett.*, vol. 27, pp. 1767–1769, 2002.

[42] J.-S. Jang and B. Javidi, "Three-dimensional synthetic aperture integral imaging," *Opt. Lett.*, vol. 27, pp. 1144–1146, 2002.

[43] M. Levoy, "Light fields and computational imaging," *IEEE Comput. Mag.*, vol. 39, no. 8, pp. 46–55, Aug. 2006.

[44] M. Daneshpanah, B. Javidi, and E. Watson, "Three dimensional imaging with randomly distributed sensors," *Opt. Exp.*, vol. 16, pp. 6368–6377, 2008.

[45] R. Schelein, M. Daneshpanah, and B. Javidi, "3D imaging with axially distributed sensing," *Opt. Lett.*, vol. 34, pp. 2012–2014, 2009.

[46] B. Javidi, S.-H. Hong, and O. Matoba, "Multidimensional optical sensor and imaging system," *Appl. Opt.*, vol. 45, pp. 2986–2994, 2006.

[47] J.-S. Jang and B. Javidi, "Three-dimensional projection integral imaging using micro-convex-mirror arrays," *Opt. Exp.*, vol. 12, pp. 1077–1083, 2004.

[48] J.-S. Jang, Y.-S. Oh, and B. Javidi, "Spatiotemporally multiplexed integral imaging projector for large-scale high-resolution three-dimensional display," *Opt. Exp.*, vol. 12, pp. 557–563, 2004.

[49] B. Javidi and Y. S. Hwang, "Passive near-infrared 3D sensing and computational reconstruction with synthetic aperture integral imaging," *IEEE/OSA J. Display Technol.*, vol. 4, no. 1, pp. 3–5, Mar. 2008.

[50] M. Cho and B. Javidi, "Three-dimensional tracking of occluded objects using integral imaging," *Opt. Lett.*, vol. 33, pp. 2737–2739, 2008.

[51] R. Martinez-Cuenca, G. Saavedra, M. Martinez-Corral, and B. Javidi, "Progress in 3-D multiperspective display by integral imaging," *Proc. IEEE*, vol. 97, no. 6, pp.1067–1077, Jun. 2009.

[52] R. Schulein, C. Do, and B. Javidi, "Distortion-tolerant 3D recognition of underwater objects using neural networks," *J. Opt. Soc. Amer. A*, vol. 27, pp. 461–468, Mar. 2010.

[53] H. Arimoto and B. Javidi, "Integral three-dimensional imaging with computed reconstruction," *Opt. Lett.*, vol. 26, no. 3, pp. 157–159, 2001.

[54] T. Okoshi, A. Yano, and Y. Fukumori, "Curved triple-mirror screen for projection-type three-dimensional display," *Appl. Opt.*, vol. 10, pp. 482–489, 1971.

[55] S. Yeom and B. Javidi, "Three-dimensional distortion-tolerant object recognition using integral imaging," *Opt. Exp.*, vol. 12, pp. 5795–5809, Nov. 2004.

[56] S. Manolache, A. Aggoun, M. McCormick, N. Davies, and S. Y. Kung, "Analytical model of a three-dimensional integral image recording system that uses circular- and hexagonal-based spherical surface microlenses," *J. Opt. Soc. Amer. A.*, vol. 18, pp. 1814–1821, Aug. 2001.

[57] L. Hongen, N. Hata, S. Nakajima, M. Iwahara, I. Sakuma, and T. Dohi, "Surgical navigation by autostereoscopic image overlay of integral videography," *IEEE Trans. Inf. Technol. Biomed.*, vol. 8, no. 2, pp. 114–121, Jun. 2004.

[58] Y. Igarishi, H. Murata, and M. Ueda, "3D display system using a computer-generated integral photograph," *Jpn. J. Appl. Phys.*, vol. 17, pp. 1683–1684, 1978.

[59] M. Martínez-Corral, B. Javidi, R. Martínez-Cuenca, and G. Saavedra, "Integral imaging with improved depth of field by use of amplitude modulated microlens array," *Appl. Opt.*, vol. 43, pp. 5806–5813, Nov. 2004.

[60] B. Lee, S. Jung, and J.-H. Park, "Viewing-angle-enhanced integral imaging using lens switching," *Opt. Lett.*, vol. 27, pp. 818–820, May 2002.

[61] J. S. Jang and B. Javidi, "Very-large scale integral imaging (VLSII) for 3D display," *Opt. Eng.*, vol. 44, no. 1, pp. 01400-1–01400-6, Jan. 2005.

[62] J.-Y. Son, S.-H. Kim, D.-S. Kim, B. Javidi, and K.-D. Kwack, "Image-forming principle of integral photography," *IEEE J. Display Technol.*, vol. 4, no. 3, pp. 324–331, Sep. 2008.

[63] A. Castro, Y. Frauel, and B. Javidi, "Integral imaging with large depth of field using an asymmetric phase mask," *Opt. Exp.*, vol. 15, pp. 10 266–10 273, 2007.

[64] S. Bagheri and B. Javidi, "Extension of depth of field in integral imaging using amplitude and phase modulation of the pupil function," in *Proc. SPIE—Int. Soc. Opt. Eng.*, Apr. 2008, vol. 6983, DOI: 10.1117/12.786887.

[65] S. Vassiliadis, E. A. Hakkennes, J. S. S. M. Wong, and G. G. Pechanek, "The sum-absolute-difference motion estimation accelerator *Proc. Euromicro Conf.*, 1998, vol. 2, pp. 559–566.

[66] J. W. Lichtman, "Confocal microscopy," *Sci. Amer.*, vol. 271, pp. 40–45, 1994.

[67] J.-H. Park, K. Hong, and B. Lee, "Recent progress in three-dimensional information processing based on integral imaging," *Appl. Opt.*, vol. 48, pp. H77–H94, 2009.

[68] M. Martínez-Corral, B. Javidi, R. Martínez-Cuenca, and G. Saavedra, "Formation of real, orthoscopic integral images by smart pixel mapping," *Opt. Exp.*, vol. 13, pp. 9175–9180, 2005.

[69] D.-C. Hwang, J.-S. Park, D.-H. Shin, and E.-S. Kim, "Depth-controlled reconstruction of 3D integral image using synthesized intermediate sub-images," *Opt. Commun.*, vol. 281, pp. 5991–5997, 2008.

[70] G. Saavedra, R. Martínez-Cuenca, M. Martínez-Corral, H. Navarro, M. Daneshpanah, and B. Javidi, "Digital slicing of 3D scenes by Fourier filtering of integral images," *Opt. Exp.*, vol. 16, pp. 17 154–17 160, 2008.

[71] H. M. Ozaktas and L. Onural, Eds., *Three-Dimensional Television: Capture, Transmission, and Display*. New York: Springer-Verlag, 2007.

[72] S. W. Min, B. Javidi, and B. Lee, "Enhanced 3D integral imaging system by use of double display devices," *Appl. Opt.—Inf. Process.*, vol. 42, pp. 4186–4195, Jul. 10, 2003.

[73] B. Javidi, S. Min, and B. Lee, "Enhanced 3D color integral imaging using multiple display devices," in *Proc. Annu. Meeting IEEE Lasers Electro-Optics Soc.*, San Diego, CA, Nov. 2001, vol. 2, pp. 491–492.

[74] A. Stern and B. Javidi, "Ray phase space approach for 3D imaging and 3D optical data representation," *IEEE J. Display Technol.*, vol. 1, no. 1, pp. 141–150, Sep. 2005.

[75] A. Stern and B. Javidi, "Information capacity gain by time-division multiplexing in 3D integral imaging," *Opt. Lett.*, vol. 30, pp. 1135–1137, 2005.

[76] R. Martinez, A. Pons, G. Saavedra, M. Martinez-Corral, and B. Javidi, "Optically-corrected elemental images for undistorted integral image display," *Opt. Exp.*, vol. 14, pp. 9657–9663, 2006.

[77] R. Martinez-Cuenca, G. Saavedra, M. Martinez-Corral, and B. Javidi, "Enhanced depth of field integral imaging with sensor resolution constraints," *Opt. Exp.*, vol. 12, pp. 5237–5242, 2004.

[78] W. Furlan, M. Martinez-Corral, B. Javidi, and G. Saavedra, "Analysis of 3D integral imaging displays using the Wigner distribution," *IEEE J. Display Technol.*, vol. 2, no. 2, pp. 180–185, Jun. 2006.

[79] R. Martinez-Cuenca, G. Saavedra, M. Martinez-Corral, and B. Javidi, "Extended depth-of-field 3-D display and visualization by combination of amplitude-modulated microlenses and deconvolution tools," *IEEE J. Display Technol.*, vol. 1, no. 2, pp. 321–327, Dec. 2005.

[80] M. Martinez-Corral, B. Javidi, R. Martinez-Cuenca, and G. Saavedra, "Integral imaging with improved depth of field by use of amplitude-modulated microlens arrays," *Appl. Opt.*, vol. 43, pp. 5806–5813, 2004.

[81] R. Hartley and A. Zisserman, *Multiple View Geometry in Computer Vision*, 2nd ed. Cambridge, U.K.: Cambridge Univ. Press, 2004.

[82] Y.-T. Lim, J.-H. Park, K.-C. Kwon, and N. Kim, "Resolution-enhanced integral imaging microscopy that uses lens array shifting," *Opt. Exp.*, vol. 17, no. 21, pp. 19 253–19 263, 2009.

[83] D. H. Shin, M. Cho, and B. Javidi, "Three-dimensional optical microscopy using axially distributed image sensing," *Opt. Lett.*, vol. 35, no. 21, pp. 3646–3648, 2010.

[84] B. Javidi, I. Moon, S. Yeom, and E. Carapezza, "Three-dimensional imaging and recognition of microorganism using single-exposure on-line (SEOL) digital holography," *Opt. Exp.*, vol. 13, no. 12, pp. 4492–4506, 2005.

[85] B. Javidi, I. Moon, and S. Yeom, "Real-time 3D sensing and identification of microorganisms," *Opt. Photon. News Mag.*, vol. 17, no. 2, pp. 16–21, 2006.

ABOUT THE AUTHORS

Myungjin Cho received the B.S. and M.S. degrees in telecommunication engineering from Pukyong National University, Busan, South Korea, in 2003 and 2005, respectively. Currently, he is working towards the Ph.D. degree in electrical engineering at the University of Connecticut, Storrs.

He worked as a Researcher at Samsung Electronics, Korea, from 2005 to 2007. His research interests are areas of digital image processing, 3-D display, 3-D signal processing, 3-D object tracking, 3-D photon-counting imaging, and 3-D underwater imaging.

Mr. Cho is the recipient of the 2010 International Society for Optical Engineers (SPIE) Scholarship.

Mehdi Daneshpanah (Member, IEEE) received the B.Sc. degree from Isfahan University of Technology, Isfahan, Iran, in 2005 and the M.Sc. and Ph.D. degrees from the University of Connecticut, Storrs, in 2007 and 2010, respectively, all in electrical engineering.

He has published 14 journal papers, two book chapters, and 17 conference presentations, three of which have been recognized with best paper awards (as author or coauthor) in major conferences. His current research interests lie in the area of computational-optical sensing and imaging, particularly, 3-D imaging and display systems including digital holographic microscopy, multiperspective passive sensing, and coded-aperture techniques.

Dr. Daneshpanah is a member of the Optical Society of America (OSA) and The International Society for Optical Engineers (SPIE) and recipient of the 2008 IEEE Lasers and Electro-Optics Society (LEOS) Graduate Fellowship Award as well as SPIE Scholarship in Optical Science and Engineering in 2008.

Inkyu Moon received the B.S. and M.S. degrees in electronics engineering from SungKyunKwan University, Seoul, South Korea, in 1996 and 1998, respectively, and the Ph.D. degree in electrical and computer engineering from University of Connecticut, Storrs, in 2007.

From January 2008 to January 2009, he was a Researcher in a postdoctoral position at the University of Connecticut. Since 2009, he has been an Assistant Professor at the School of Computer Engineering, Chosun University, Gwangju, South Korea. His research interests include digital holography, optical information processing, computational integral imaging, optical and digital encryptions, 3-D digital image processing, 3-D statistical pattern recognition, and 4-D tracking algorithms.

Bahram Javidi (Fellow, IEEE) received the B.S. degree from the George Washington University, Washington, DC, in 1980 and the M.S. and Ph.D. degrees from the Pennsylvania State University, University Park, in 1982 and 1986, respectively, all in electrical engineering.

He is the Board of Trustees Distinguished Professor at the University of Connecticut, Storrs. He has over 630 publications. He has published over 290 technical articles in major peer-reviewed journals. He has published over 330 conference proceedings, including over 110 plenary addresses, keynote addresses, and invited conference papers. His papers have been cited over 6200 times according to the citation index of *WEB of Science* ($h-$index $= 42$). He is a coauthor on seven best paper awards.

Dr. Javidi is Fellow of seven national and international professional scientific societies, including the American Institute for Medical and Biological Engineering (AIMBE), the Optical Society of America (OSA), and The International Society for Optical Engineers (SPIE). In 2008, he received a Fellow award by John Simon Guggenheim Foundation. In 2010, he was the recipient of The George Washington University's Distinguished Alumni Scholar Award, University's highest honor for its alumni in all disciplines. He received the 2008 IEEE Donald G. Fink prized paper award among all (over 130) IEEE Transactions, Journals, and Magazines. In 2007, The Alexander von Humboldt Foundation awarded Dr. Javidi with Humboldt Prizes for outstanding U.S. scientists. He received the Technology Achievement Award from SPIE in 2008. In 2007, he was the corecipient of the best paper award from the Information Optics workshop sponsored by the IEEE Lasers and Electro-Optics Society (LEOS), SPIE, and University of Iceland. In 2005, he received the Dennis Gabor Award in Diffractive Wave Technologies by SPIE. He was the recipient of the IEEE LEOS Distinguished Lecturer Award twice in 2003–2004 and 2004–2005. He was awarded the IEEE Best Journal Paper Award from the IEEE TRANSACTIONS ON VEHICULAR TECHNOLOGY twice in 2002 and 2005. In 1990, the National Science Foundation named Prof. Javidi a Presidential Young Investigator. In 1987, he received The Engineering Foundation and the IEEE Faculty Initiation Award. He was selected in 2003 as one of the nation's top 160 engineers between the ages of 30–45 by the National Academy of Engineering (NAE) to be an invited speaker at The Frontiers of Engineering Conference which was cosponsored by The Alexander von Humboldt Foundation. He has been an alumnus of the Frontiers of Engineering of The National Academy of Engineering since 2003. He is on the Editorial Boards of the PROCEEDINGS OF THE IEEE, the IEEE/OSA JOURNAL OF DISPLAY TECHNOLOGY, and *SPIE Reviews*.